International Journal of Enhanced Research in Science, Technology & Engineering
ISSN: 2319-7463, Vol. 5 Issue 2, February-2016

Design of an Robust Controller for Positioning of Azimuth-Elevation-Tilt Pedestals in Low Elevation Orbit Satellite Tracking Missions

Mahmud Salamati[1], Mostafa Sarlak[2], Abbas Mirzaie[3]

[1,2,3]Research Assistant, Electrical and Computer Engineering Department, University of Tehran, Tehran, Iran

ABSTRACT

Satellite tracking stations (STSs) are used in order to track satellite over a specified range of positions. Pedestals are being used as the most important component in each STS. Elevation over azimuth (Az-Elv) pedestals are the most common type of the pedestals, which are used in order to track low elevation orbit (LEO) satellites. However, due to motor speed limit, Az-Elv pedestals are unable to track targets at high elevations near the zenith point. Azimuth-Elevation-Tilt (Az-El-Ti) can overcome this problem by introducing a third degree of freedom. However, there still remains real challenges in tracking targets under disturbances such as high speed winds. Considering conventional proportional-integral (PI) controllers, the overall system suffers from poor tracking performance under load variations. Moreover, the mechanical characteristics of load such as viscous coefficient and moment of inertia vary gradually. It is a key feature for drive controller to be robust against all these changes. This paper presents a solution for efficient performance of Az-El-Ti pedestals in terms of accurate positioning even during passing the zenith point. The most important advantage of the introduced controller is its non-sensitivity to the variations of load, moment of inertia and viscous coefficient. The controller output will regulate the output position of pedestal's actuators. Permanent magnet synchronous motors (PMSMs) are taken into consideration as the best choice for satisfaction of control objectives. Then a robust sliding mode controller is designed via defining suitable sliding surface and calculating the corresponding control input. While the designed controller is regulating the q-axis current of a PMSM motor, the tracking accuracy is measured via simulating, considering an accurate, nonlinear model of the motor. At last, the controller's performance is validated when it is used in an Az-El-Ti pedestal and the wind is blowing with different speed profiles. The reference azimuth and elevation data are chosen from a real tracking mission and simulation results prove effectiveness of the proposed approach for controlling LEO pedestals.

Keywords: , Sliding mode controller, azimuth-elevation-tilt pedestal, LEO satellite track, PMSM drive.

I. INTRODUCTION

Pedestals are in charge of placing the antenna in a position at which, receiving telemetry data from satellite is performed with the best quality. Losing accuracy in antenna positioning will result in loss of significant amount of data [1]. Satellites circulate in different orbits with distinct elevations relative to the earth. LEO satellites offer some benefits in comparison with their geostationary earth orbit (GEO) cousins [2]. Having lower launch costs, less power requirements and reduced roundtrip transmission delay, compared to a GEO, makes LEOs more appropriate satellites. Moreover, in contrast with GEO constellations which only can see earth stations with latitudes less than 81°, a LEO constellation is capable to communicate with all points on the globe, using the polar orbits.

Satellite tracking stations (STS) must be capable of tracking satellites in specified range of positions. There are different kinds of pedestals which are used to track satellites. Pedestals which are used in LEO STSs are categorized according to their degrees of freedom. The most prevalent type of pedestals is the elevation over azimuth pedestal (Az-Elv pedestals) [3]. The most important advantage of these pedestals is that their reference position is easily provided. In fact, telemetry data which are being sent by the target satellite, contain the satellite's position in terms of azimuth and elevation angles. Therefore, there is no need for any additional conversion of these data. The pedestal has to rotate and move its reflector to be placed at a point with received azimuth and elevation.

Whatever the telemetry data signal is stronger, the quality of the data reception goes higher. In other words, when satellite is located in higher altitudes, the quality of the received signal reduces. Zenith point is a position at which, the pedestal's reflector is in horizontal state and satellite is crossing from the top of the pedestal, i.e., the elevation angle of the satellite is going to decrease from 90°. At this instant, the azimuth angle of pedestal has to be changed 180° in a short time period because the elevation motor is only allowed to rotate at angles between 0 and 90. This is very important that

the station can be capable of continuing a good tracking through and near the local zenith to assure quality reception of the telemetry data [4]. To reduce the high speeds of Azimuth motor in zenith pass and to avoid signal loss in the "dead zones" pedestals with 3-axes Support-Rotating Device (SRD) with an implemented additional azimuth axis of E1 with a slope $\gamma = 15°$ are developed.

Az-El-Tilt are capable of removing main problem of traditional Az-Elv pedestals, enabling high quality data reception during zenith pass. However, there are still a number of significant challenges in accurate positioning of these pedestals. The diameter of reflector body varies up to several meters. Significant torques should be supplied by servo mechanism in order to move the reflector. However, the amount of required torque is not constant at different positions. Moreover, STSs are mostly placed on top of hills where the wind speed is higher in comparison with near the earth surface. It is not easy for actuator control system of pedestals to maintain high accuracy in positioning under load variations. Regarding variations of wind speed and weight generated load torque in different elevation angles, so it is very important to design a controller which is able to overcome load changes.

Figure 1. Az-El- Tilt pedestal

As it was stated before, finding a solution for accurate positioning of Az-El-Tilt pedestal's antenna seems to be of high importance. Electric motors are in charge of putting the pedestal's reflector in the desired point. Therefore, it is important to choose the best kind of electric motor and design its drive carefully. Permanent magnet synchronous motors (PMSMs), are being used widely in many application due to possessing characteristics such as high power density, torque-to-inertia ratio, and efficiency. Linear control schemes such as LQR based pole placement and proportional integral (PI) controllers are mostly being used to control PMSM's position and speed. Different types of linear controller including LQR and H∞ control schemes are suggested in [5]-[9]. These methods cannot offer good pointing accuracy because of inherent limitations in linear controllers' performance. However, the PMSM servo system is a nonlinear system with unavoidable and unmeasured disturbances, as well as parameter variations [10]. This makes it very difficult for linear control algorithms to obtain a sufficiently high performance for this kind of nonlinear systems. In fact, these schemes are easy from implementation perspective. On the other hand, it is verified that LQR position control results in steady state error in case of load changes. Similarly, PI controllers causes that system shows a relative long period of transients in output position when load changes. In Az-El-Tilt pedestal application, load is continuously being changed. Therefore, it is a must to design a robust controller, such that fluctuations on their shaft position will be removed.

With regards to nonlinear model of PMSMs, Nonlinear control algorithms become an appropriate solution for controlling these motors. Recently, with the rapid progress in power electronics, microprocessors, especially digital signal processors (DSPs), and modern control theories, many researchers have aimed to develop nonlinear control methods for the PMSM, and various algorithms have been proposed, e.g., adaptive control [10-12], robust control [13], sliding-mode control [14], [15], input–output linearization control [16], backstepping control [17-18], and intelligent control [19]. These algorithms have boosted the performance of PMSM from different aspects.

In this paper, we have considered PMSM as the Az-El-Tilt pedestal's actuator. The paper continues with a description of Pedestal actuators' modeling. In the next parts, the proposed sliding mode controller design is described and its performance is compared with PI and LQ state feedback control schemes. In the final section, the whole Az-El-Tilt pedestal system using the designed adaptive controller is simulated under real conditions and results prove high robustness of the proposed sliding mode controller in accurate positioning under high load variations.

II. MODELLING THE PEDESTEL's ACTUATORS

Among all pedestal's constituents, electrical motors are the most important component to be modeled due to their nonlinear dynamics and their role in pointing. PMSMs seem to be the best choice according to their high efficiency, having compact construction and less maintenance costs in comparison with induction and direct current motors. Moreover, they are able to produce a ripple free torque in comparison with the Brush Less DC motors.

Taking the rotor coordinates (d−q axes) of the motor as reference coordinates, the model of a surface-mounted PMSM motor can be described as

$$\begin{pmatrix} \dot{i}_d \\ \dot{i}_q \\ \dot{\omega}_m \end{pmatrix} = \begin{pmatrix} -\frac{R}{L} & n_p\omega_m & 0 \\ -n_p\omega_m & -\frac{R}{L} & \frac{n_p\varphi_f}{L} \\ 0 & -\frac{k_t}{J_m} & -\frac{B_m}{J_m} \end{pmatrix} \begin{pmatrix} i_d \\ i_q \\ \omega_m \end{pmatrix} + \begin{pmatrix} \frac{u_d}{L} \\ \frac{u_q}{L} \\ -\frac{T_L}{J_m} \end{pmatrix} \quad (1)$$

Where

i_d , i_q d- and q-axis stator currents, respectively;

u_d , u_q d- and q-axis stator voltages, respectively;

n_p number of pole pairs;

R stator resistance;

L stator inductance;

φ_f rotor flux linkage;

K_t torque constant;

ω_m angular velocity;

B_m viscous friction coefficient;

J_m moment of inertia;

T_L load torque.

The specifications of the PMSM are shown in Table (1).

Table I. Value of the selected PMSM model parameters

rated power	750W
rated speed	3000 rpm
rated voltage	105V
rated current	4.7A
rated torque	2.3Nm
stator inductance (L)	4mH
stator resistance (R)	1.74Ω
torque constant (K_t)	1 Nm/A
rotor inertia (J)	.001 Kg× m^2/rad
viscous coefficient (B)	.0015 Nms/rad
pole pairs (n_p)	4

III. POSITION CONTROLLER DESIGN

A. *General control scheme*

The primary principle in controlling a PMSM drive is based on field orientation technique. Since the magnetic flux generated from the PM rotor is fixed in relation to the rotor shaft position, the flux position in the *d*-*q* coordinates can be determined by the shaft position sensor. If $i_d = 0$ the *d*-axis flux λ_d is fixed. Since magnetizing inductance and current are constant for a PMSM, the electromagnetic torque, T_e is then proportional to i_q, which is determined by closed-loop control. The rotor flux is produced only in the *d* axis while the current vector is generated in the *q* axis in the field-oriented control. Since the generated motor torque is linearly proportional to the *q*-axis current as the *d*-axis rotor flux is constant, the maximum torque per ampere can be achieved.

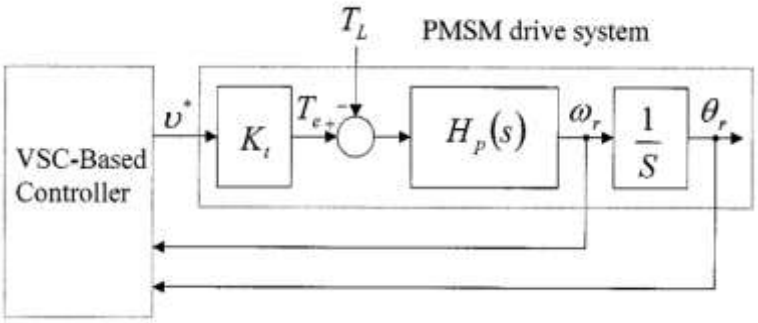

Figure 2. Simplified control system block diagram.

The configuration of a field-oriented PMSM drive system with conventional cascade position and speed control is shown
in Fig. 2. The PMSM used in this drive system is a three-phase four-pole 750-W 4.7-A 3000-r/min type. Using the field-oriented mechanism, the PMSM drive system can be simplified to the control system block diagram shown in Fig. 2, in which

$$T_e = K_t v \tag{2}$$

$$H_p(s) = \frac{1}{J_m s + B_m} \tag{3}$$

The parameters of the experimental servo motor system in its nominal condition are $K_t = 1\,{}^{N.m}/_{A}$, $J_m = 0.001 N.m \times s^2/rad$ and $B_m = 0.0015 N.m \times s/rad$. In addition, v is the inverter torque command which is proportional to the *q*-axis current i_q.

In this section, based on the state-space equation of the motor dynamic system and the introduced performance index, the general concepts of LQ method will be described. Thereafter, under the obtained feedback gain, a new robust controller will be developed to conserve the control performance designed by the LQ method.

B. *Nominal condition*

To design a desired controller using the LQ method, the system must first be expressed in the state-space form. Considering the electromechanical equations of the motor, with taking external load into consideration we will have

$$\begin{bmatrix} \dot{\theta_m} \\ \dot{\omega_m} \end{bmatrix} = \begin{bmatrix} 0 & 1 \\ 0 & -\frac{B_m}{J_m} \end{bmatrix} \begin{bmatrix} \theta_m \\ \omega_m \end{bmatrix} + \begin{bmatrix} 0 \\ \frac{1}{J_m} \end{bmatrix} T_e - \begin{bmatrix} 0 \\ \frac{1}{J_m} \end{bmatrix} T_L \tag{4}$$

For position control, we redefine the new state variables x_1 and x_2 as

$$\begin{cases} x_1 = \theta_m - \theta_d \\ x_2 = \omega_m \end{cases} \tag{5}$$

where θ_d denotes the position command. Then, combining (4) with (5), the following new state-space equation without considering the disturbance is obtained:

$$\dot{X} = AX + bv = \begin{bmatrix} 0 & 1 \\ 0 & a \end{bmatrix} X + \begin{bmatrix} 0 \\ b \end{bmatrix} v \tag{6}$$

where $a = \frac{-B_m}{J_m}$, $b = \frac{K_t}{J_m}$, and $X^T = [x_1\ x_2]$ is the state. In view of the LQ method, it is to find an optimal control, v^*, minimizing the performance index *J*

$$J = \int_0^\infty (X^T Q X + v^T R V)\, dt \tag{7}$$

associated with the system (6). In (7), matrix **R** is positive definite, and **Q** is nonnegative definite. To find the optimal control law, v^*, the following Riccati equation:

$$A^T P + PA - PbR^{-1}b^T P + Q = 0 \tag{8}$$

is first solved. Let $\bar{P}$ be the solution for (8) and be nonnegative. Thus, to yield a minimum index of (7), the control law is as follows:

$$v^* = -K^T X = -(R^{-1}b^T \bar{P})^T X \tag{9}$$

and the feedback gain is defined as

$$K = R^{-1}b^T \bar{P} \tag{10}$$

When system (6) is under the control of (9), the resultant closed-loop dynamics are given by

$$\dot{X} = [A - bK^T]X = A_c X \tag{11}$$

C. *New Sliding Surface*

Here, a new switching function for sliding-mode position control is designed as follows:

$$\sigma(x,t) = C^T[X - X_0] - C^T A_C \int_0^t X(\tau) d\tau = 0 \tag{12}$$

Where **X** is system state and X_0 is its initial value. In addition, A_C is a constant vector, which is chosen to make (12) simple but satisfies $C^T b \neq 0$. The choice for the current condition is $C^T = [0\ \ {}^1/_b]$, then $C^T b = 1$. It is obvious that, based on (12), $\sigma(X,t) = 0$ during all the control process. Therefore, for any chosen state feedback (9), the system possesses a sliding surface $\sigma(X,t) = 0$ on which the state slides.

D. *Real Condition*

For most of the system, the perturbation exists, then the linear optimal control v^* in (9) will neither minimize the performance index (7) nor maintain the sliding mode, $\sigma(X,t) = 0$. Thus, the desired performance will be deteriorated and the steady-state error will occur. To overcome the drawbacks of the LQ method, a VSC-based strategy will be added to the conventional LQ-method-based control system.
For a more realistic condition, the nominal system (6) is rewritten as

$$\dot{X} = (A + \Delta A)X + (B + \Delta B)\vartheta + d = \begin{bmatrix} 0 & 1 \\ 0 & a + \Delta a \end{bmatrix} X + \begin{bmatrix} 0 \\ b + \Delta b \end{bmatrix} v + d \tag{13}$$

where ΔA and Δb denote the uncertainties introduced by system parameters J_m, B_m, and K_t , and **d** represents the external disturbance and its form is as

$$d = \begin{bmatrix} 0 \\ d \end{bmatrix} = \begin{bmatrix} 0 \\ \frac{T_L}{J_m} \end{bmatrix} \tag{14}$$

Equation (13) can be expressed in the form of

$$\dot{X} = AX + bv + P \tag{15}$$

Where **P** is the total perturbation given by

$$p = \Delta A X + \Delta b v + d \tag{16}$$

For the position control system, **P** vector is of the form

$$P = \begin{bmatrix} 0 \\ P \end{bmatrix} \tag{17}$$

Then, (16) can be rewritten in scalar form as

$$p = \Delta a x_2 + \Delta b v + d \tag{18}$$

One's object is to keep the system states on the sliding surface. Once the sliding mode $\sigma(X,t)=0$ can be obtained during all the control process, the control system will reserve as an equivalent system whose dynamics are the same as the closed-loop dynamics in the nominal condition given by (11). To reserve the nominal responses and control the states on the sliding surface under the perturbed condition, a new control is given as

$$\bar{V}^* = V^* - q.sgn(\sigma) = -K^T X - q.sgn(\sigma) = -k_1 x_1 - k_2 x_2 - q.sgn(\sigma) \tag{19}$$

where **sgn(.)** is a sign function defined as

$$sgn(\sigma) = \begin{cases} +1, & if\ \sigma > 0 \\ -1, & if\ \sigma < 0 \end{cases} \tag{20}$$

σ has been defined in (12) and q is defined as the upper bound of the total perturbation (17), i.e.,

$$\left|\frac{p}{b}\right| \le q \tag{21}$$

Lemma: If the switching surface $\sigma(X,t)$ of the controlled system satisfies the following condition, then the existent condition of the sliding mode, $(X,t)=0$, must be guaranteed **[10]**

$$\sigma\dot{\sigma} < 0 \tag{22}$$

Theorem: The position control given by (19) makes the sliding mode occur and stabilizes the system (13).
Proof: According to the lemma, the existence of the sliding mode of the proposed control can be derived as

$$\begin{aligned} \sigma\dot{\sigma} &= \sigma\left[\frac{1}{b}\dot{x_2} + k_1 x_1 + \left(k_2 - \frac{a}{b}x_2\right)\right] \\ &= \sigma\{\tfrac{1}{b}[(a+\Delta a)x_2 + (b+\Delta b)v^*] + k_1 x_1 + \left(k_2 - \tfrac{a}{b}x_2\right)\} \end{aligned} \tag{23}$$

Replacing the control input v^* with (19), one can obtain the following inequality:

$$\sigma\dot{\sigma} \le \sigma[\tfrac{p}{b} - q\ sgn(\sigma)] \le 0 \tag{24}$$

Therefore, using the control law (19), the existent condition of the sliding mode in the lemma is satisfied, and the dynamic of the closed-loop system is governed by (11), which is designed stable, so that state X(t) will slide into the origin.

Remark: Because the system is in the sliding mode for the controlled period, the state responses of perturbed system (13) will be totally the same as desired system (17), i.e., it is invariant all the time.

E. *Simulation results for PMSM response*

In this section, it is intended to verify the controller's performance in satisfying the tracking goals of individual permanent magnet synchronous motors. The motor's characteristics are the same as the Table. I parameters. Simulations are done in MATLAB environment and the detailed nonlinear dynamics of the motors are considered for modelling purposes. The controlled object is to drive the motor rotor to rotate 0.5235 rad, which is about 30°. The parameters of the PMSM drive system in nominal condition have been given in previous Sections, and substituting them into (6), we have the state-space equation as

$$\begin{bmatrix} \dot{x_1} \\ \dot{x_2} \end{bmatrix} = \begin{bmatrix} 0 & 1 \\ 0 & -1.5 \end{bmatrix} \begin{bmatrix} x_1 \\ x_2 \end{bmatrix} + \begin{bmatrix} 0 \\ 1000 \end{bmatrix} v - \begin{bmatrix} 0 \\ 1000 \end{bmatrix} T_L \tag{25}$$

To determine the feedback gain **K** for PMSM drive system, matrices **Q** and **R** in (7) are chosen as

$$Q = \begin{bmatrix} 100 & 0 \\ 0 & 5 \end{bmatrix} \qquad \text{R=70} \tag{26}$$

and the resultant feedback gain is $K^T = [1.1952\ 0.2702]$. The poles of the closed-loop dynamic system are at -4.472 and -267.228, respectively. To reduce the chattering of the SMC, the smooth function is utilized in the control law (19), i.e.,

$$\bar{v}^* = -K^T X - q\frac{\sigma}{|\sigma|+\delta} \tag{27}$$

Where δ is a small positive constant chosen as 0.01.

As it was stated before, proportional integral (PI) controllers are used widely in order to control permanent magnet SMs. Fig. 3 shows a conventional position control scheme using PI position, speed and current controllers.

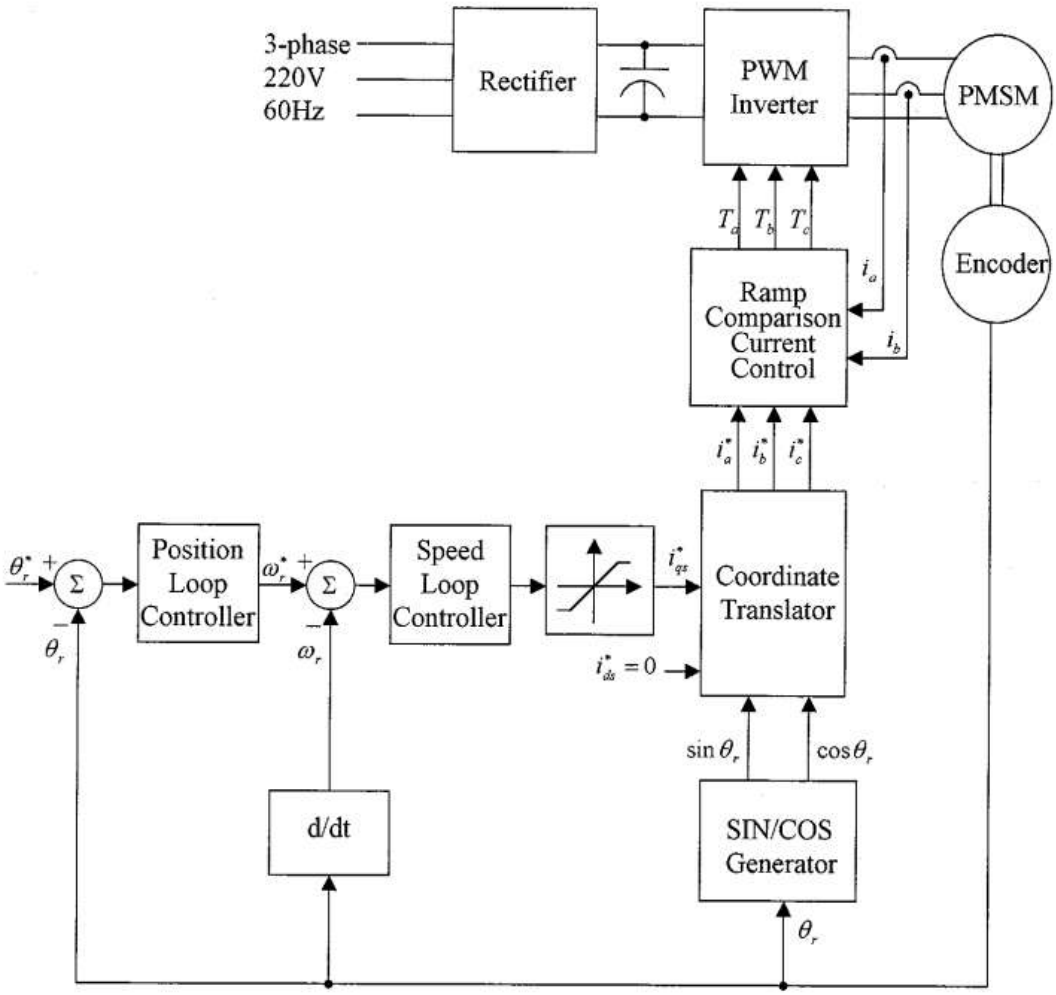

Figure 3. Conventional position control scheme for PMSMs using PI controllers

The PI controller gains for position, speed and d and q current controllers has been shown in the table (2).

TABLE 2. PI GAINS FOR POSITION AND CURRENT CONTROLLERS

Kp(position controller)	10
Ki(position controller)	1
Kp(speed controller)	.8
Ki(speed controller)	1.25
Kp(current controllers)	40
Ki(current controllers)	2500

In the following, effects resulting from the external disturbances are given in Fig. 4. In those simulated results, a 2 N.m load is suddenly added to the position control system at time 2 s. It is obvious that the position response caused by the LQ method shows a steady-state error. The PI controller removes steady state error; however, response is highly influenced after introducing a sudden load torque. But, the steady-state error is zero for the system based on the sliding mode controller and moreover system performance seems to be independent of load changes. Observing the responses controlled by the proposed new one, choosing an appropriate extra control force *q*, the system response is independent of the disturbance as Fig. 4 shows. Above all, the response is the same as that of the nominal system before and after the load is added. It is proved that the system controlled by the proposed robust controller is invariant to the disturbance.

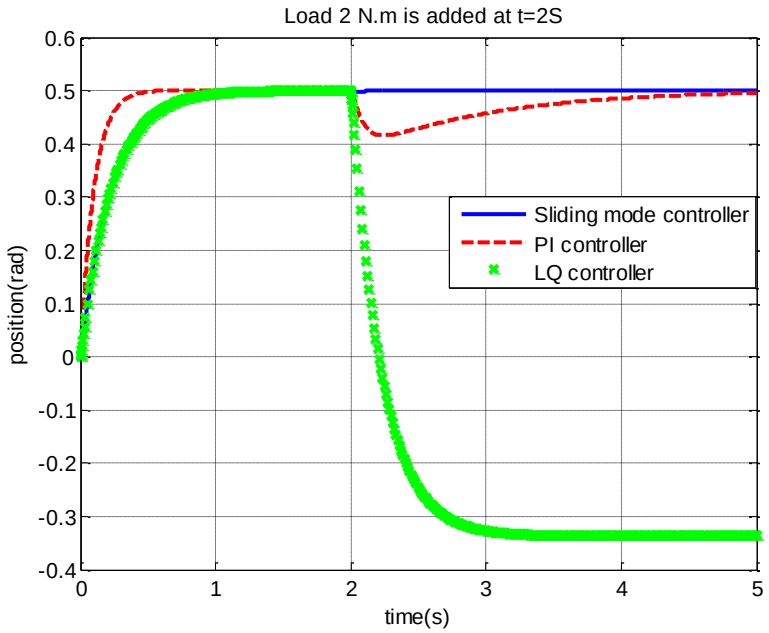

Figure 4. Comparison between performance of PMSM position tracking in presence of a load adding by SLM, LQ and PI controllers

Another consideration for the proposed new optimal controller is that this new one just exists in the sliding phase but not in the reaching phase. i.e., the system controlled by this new one is robust and invariant from the beginning of the control process. A load with 2.0 N.m is added at time 0 s and is removed at time 2 s to evaluate this property. Fig. 5 shows the results under this condition. The system controlled by the LQ method and LQ method with integral feedback is affected at these two instants. However, the system controlled by the proposed method is still little affected; it shows a good property of robustness in the beginning and during all the control process.

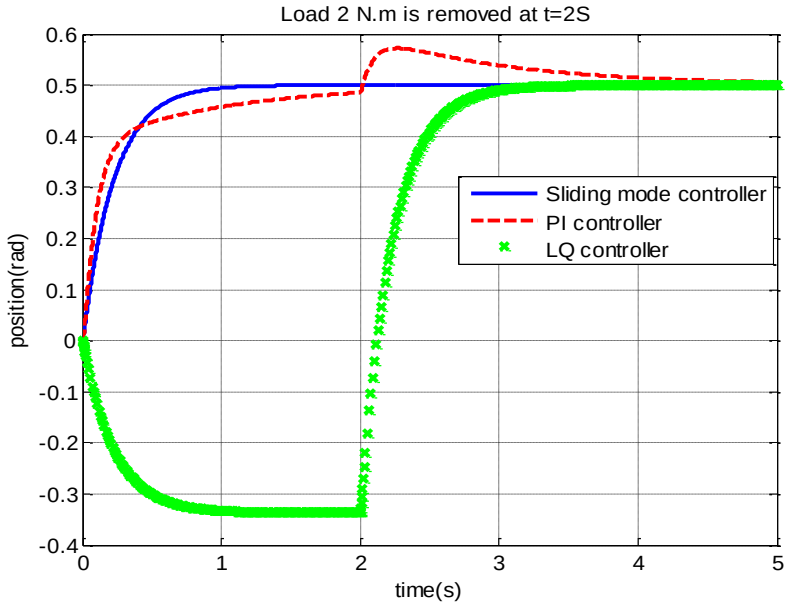

Figure 5. Comparison between performance of PMSM position tracking in presence of a load removing by SLM, LQ and PI controllers

In bellow, a schematic diagram of the PMSM control system is brought.

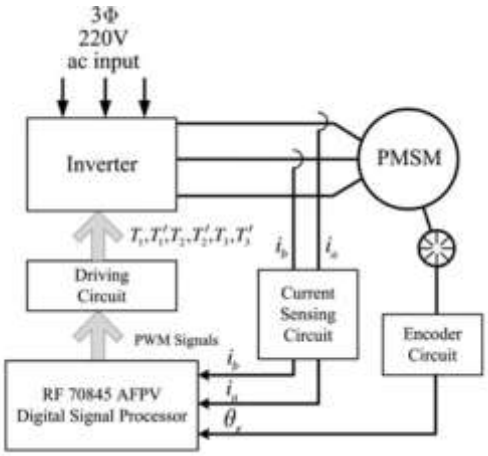

Figure 6. full diagram of a PMSM drive implementation

4. Analysis of applied forces to the pedestal

As it was discussed, an Az-El-Tilt pedestal system uses three motors in order to overcome the resistant forces and reach the reflector to any desired position in azimuth and elevation. The load torque is composed of two kinds of forces: the gravitational force which depends on the weight amount of the reflector and pedestal's back structure; and the wind force that varies with the wind speed. As the pedestal is the case, both of these forces vary when the reflector turns around in different angles.

The elevation angle has a direct impact on the amount of both gravitational and wind forces. When the reflector is placed in a horizontal position, the applied torque is approximately negligible. As the Elevation angle goes towards 0 degrees, the amount of both gravitational and wind force increase. The equation (19) models the gravitation force which is applied on the elevation motor in terms of elevation angle:

$$F_{motor-El}^{gravity} = \left(M_{pedestal} + M_{back\ structure}\right).g.\mathrm{Cos}\ (\theta_{El}) \tag{28}$$

It should be noticed that, no force would be applied to the azimuth motor from the gravitational source (Eq. 29).

$$F_{motor-Az}^{gravity} = 0 \tag{29}$$

However, because the third axis has a slope of γ relative to the direct Azimuth axis, a fraction of the total weight will resist with its rotation:

$$F_{motor-Tilt}^{gravity} = \left(M_{pedestal} + M_{back\ structure}\right).g.\mathrm{Sin}(\gamma)$$

Assuming a length of L for distance between motor shaft and the center of the reflector, we have:

$$\tau_{motor\mathrm{El}}^{gravity} = \left(M_{pedestal} + M_{back\ structure}\right).g.L_1.\mathrm{Cos}\ (\theta_{El}) \tag{30}$$

$$\tau_{motor-Tilt}^{gravity} = \left(M_{pedestal} + M_{back\ structure}\right).g.L_2\mathrm{Sin}\ (\gamma)$$

Equation (22) gives a general description of the wind force in terms of several parameters:

$$F_{wind} = \frac{1}{2}\rho A_f C_D (V + V_{wind})^2 \tag{31}$$

Where

ρ, is the air density

A_f, is the effective area of the reflector in m^2

C_D, is the aerodynamic coefficient

V, is the reflector's speed in $^m/_s$

V_{wind}, is the wind speed in $^m/_s$

The effective area of the reflector changes as the elevation angle varies. Moreover, the wind force's sign could be changed depending on the azimuth angle of the reflector and wind blowing direction. Here, we assume that wind blowing direction is always horizontally to area of the reflector. Therefore, the applied torque on elevation motor which its source is the wind can be yield through the below relationship:

$$\tau_{motor-El}^{wind} = \begin{cases} \left(\frac{1}{2}\rho A_f C_D (V + V_{wind})^2\right).L_2.\left(\frac{90-\theta_{El}}{90}\right).\sin(\theta_{El}) & 0 < \theta_{El} < 90 \\ -\left(\frac{1}{2}\rho A_f C_D (V + V_{wind})^2\right).L_2.\left(\frac{90-\theta_{El}}{90}\right).\sin(\theta_{El}) & 90 < \theta_{El} < 180 \end{cases} \tag{32}$$

Where, θ_{El} is the elevation angle. The applied torque on the azimuth and tilt motors are negligible. The overall applied torque to each of the motors can be calculated by adding the gravitational and wind torques separately.

IV. PEDESTAL CONTROL SYSTEM

LEO pedestals are used in order to track a signal source continuously. The desired position of the reflector is sent to the central controller unit in terms of reference azimuth and elevation commands. In the next step, desired position of three motors are calculated through the results of denavit-hartenberg transformation. A typical diagram of the pedestal's control system is shown in the Fig. 7.

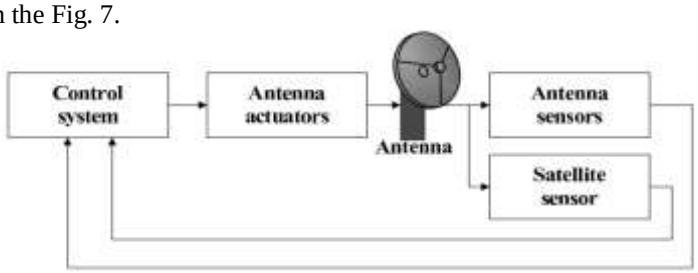

Figure 7. Schematic view of an Az-Elv pedestal's control system

The control system needs to perform the transformation of input coordinates α_j , β_j in order to accompany the spacecraft with this antenna, from a topocentric azimuth-elevation coordinate system into the local coordinate system of each axis of the pedestal (array R[t_j,α_{1j} , α_{2j} , α_{3j}]), where α_{1j}, α_{2j}, α_{3j} are the rotation angles of each axis tilt, elevation and azimuth respectively at time t_j.

$$\alpha 2 = arctg\left(\frac{\cos\gamma\cdot\sin\beta-\sin\gamma\cdot\cos\beta\cdot\cos(\alpha-\alpha 3)}{\sqrt{1-(\cos\gamma\cdot\sin\beta-\cos\beta\cdot\cos(\alpha-\alpha 3)\cdot\sin\gamma)^2}}\right)+\gamma$$

$$\alpha 1=\begin{cases}\alpha_1', \text{ if } X_A\geq 0;\\ \alpha_1'+180^\circ, \text{ if } X_A<0 \text{ and } Z_A\geq 0;\\ \alpha_1'-180^\circ, \text{ if } X_A<0 \text{ and } Z_A<0;\end{cases}$$

$$\alpha_1' = arctg\left(\frac{\cos\beta\cdot\sin(\alpha-\alpha 3)}{\cos\gamma\cdot\cos\beta\cdot\cos(\alpha-\alpha 3)+\sin\gamma\cdot\sin\beta}\right)$$

$$X_A=\cos\gamma\cdot\cos\alpha 3\cdot\cos\alpha\cdot\cos\beta+\sin\gamma\cdot\sin\beta+\cos\gamma\cdot\sin\alpha 3\cdot\cos\beta\cdot\sin\alpha\,,$$

$$Y_A=-\sin\gamma\cdot\cos\alpha 3\cdot\cos\beta\cdot\cos\alpha+\cos\gamma\cdot\sin\beta-\sin\gamma\cdot\sin\alpha 3\cdot\cos\beta\cdot\sin\alpha\,,$$

$$Z_A=-\sin\alpha 3\cdot\cos\beta\cdot\cos\alpha+\cos\alpha 3\cdot\cos\beta\cdot\sin\alpha\,, \qquad (33)$$

α_1– the rotation angle of the tilt axis E1,
α_2 – the rotation angle of the elevation axis E2, and
α_3 – the rotation angle of the azimuth at vertical axis E3.
$\gamma \cong 15°$- the angle of the axis E1 relative to the axis of E3.
The range of angle limits are as bellow:
α- (0 to 360°),
β- (0 to 90°),
α_1, α_3 - (-170° to 170°),
α_2 - (0 to 120°).
During the execution of the accompaniment of a spacecraft with a given aimer table (array R[t_j,α_j , β_j]), the controller control system has to convert them into a format of local coordinates (array R[t_j,α_{1j} , α_{2j} , α_{3j}]).
To determine the real data about the AS's position and to compare with a given aimer table and issue them in the control and information processing unit, it is necessary that the inverse transformation of the "local" coordinate axes in the system topocentric coordinates pointing to the spacecraft accord with the correspondences below:

$$\alpha=\begin{cases}\alpha', \text{ if } X_B\geq 0,\ Z_B\geq 0;\\ \alpha'+360^\circ, \text{ if } X_B\geq 0 \text{ and } Z_B<0;\\ \alpha'+180^\circ, \text{ if } X_B<0;\end{cases}$$

$$\alpha' = arctg\left(\frac{\cos\gamma\cdot\sin\alpha3\cdot\cos(\alpha2-\gamma)\cdot\cos\alpha1-\sin\gamma\cdot\sin\alpha3\cdot\sin(\alpha2-\gamma)+\cos\alpha3\cdot\cos(\alpha2-\gamma)\cdot\sin\alpha1}{\cos\gamma\cdot\cos\alpha3\cdot\cos(\alpha2-\gamma)\cdot\cos\alpha1-\sin\gamma\cdot\cos\alpha3\cdot\sin(\alpha2-\gamma)-\sin\alpha3\cdot\cos(\alpha2-\gamma)\cdot\sin\alpha1}\right)$$

$$X_B = \cos\gamma\cdot\cos\alpha3\cdot\cos(\alpha2-\gamma)\cdot\cos\alpha1-\sin\gamma\cdot\cos\alpha3\cdot\sin(\alpha2-\gamma)-\sin\alpha3\cdot\cos(\alpha2-\gamma)\cdot\sin\alpha1;$$

$$Y_B = \sin\gamma\cdot\cos(\alpha2-\gamma)\cdot\cos\alpha1+\cos\gamma\cdot\sin(\alpha2-\gamma);$$

$$Z_B = \cos\gamma\cdot\sin\alpha3\cdot\cos(\alpha2-\gamma)\cdot\cos\alpha1-\sin\gamma\cdot\sin\alpha3\cdot\sin(\alpha2-\gamma)+\cos\alpha3\cdot\cos(\alpha2-\gamma)\cdot\sin\alpha1$$

$$\beta = arctg\left(\frac{\cos\gamma\cdot\sin(\alpha2-\gamma)+\sin\gamma\cdot\cos(\alpha2-\gamma)\cdot\cos\alpha1}{\sqrt{1-(\sin\gamma\cdot\cos(\alpha2-\gamma)\cdot\cos\alpha1+\cos\gamma\cdot\sin(\alpha2-\gamma))^2}}\right)$$

(34)

The control system of such an AS needs to calculate and execute the required angle α_3 vertical azimuth axis E3 after every calculation or after receiving - via the communication channel - the trajectory of spacecraft, taking into account the mechanical limits of the rotation range of this axis, as follows:

$$\alpha3 = \alpha_M, \text{ if } 0 \le \alpha_M \le \alpha_{\theta^+};$$

$$\alpha3 = \alpha_{\theta^+}, \text{ if } \alpha_{\theta^+} < \alpha_M \le 180°;$$

$$\alpha3 = \alpha_{\theta^-}, \text{ if } 180° < \alpha_M < 190°;$$

$$\alpha3 = \alpha_M - 360°, \text{ if } 360° + \alpha_{a^-} \le \alpha_M \le 360°;$$

(35)

where:

$\alpha_{\theta+}$, $\alpha_{\theta-}$ are the angles of triggering the limit switches the constraint turn of the antenna on the angle α_3 (around the tilt axis E3) into "plus" and "minus" respectively ($\alpha_{\theta+} = 170°, \alpha_{\theta-} = -170°$)

α_M is a value of azimuth counting with a maximum angle of the elevation of the spacecraft ($\alpha_M = \alpha(t)$ at $\beta(t) = \beta_{max}$), determined from the pointing-table that is calculated for the selected spacecraft.

The heart of the control system, is consisted of three PMSM robust sliding mode position controllers. The controllers' equations were described in detail in the former sections.

V. AZ-EL_TILT ROBUST SLIDING MODE CONTROL SIMULATION RESULTS

In the last sections, a complete model of pedestal's components and applied forces were extracted and the controllers' equations were explained in detail. In this section we have used a set of real azimuth and elevation data and the results of implementing the designed controllers has been studied. The table (3) shows the value of parameters of the simulated pedestal system.

Table 3. Parameters for a typical pedestal and controller gains

Parameter	Value	Parameter	Value
ρ	1.2	Wind speed	90 km/h
C_D	0.3	Mass of reflector and back structure	501.78 kg
J	1.78×10^{-4}	Gravity constant	$9.81\ \frac{m}{s^2}$
Reflector's radius	150cm	Motor's inductance	4mH
B	0.000074 Nms/rad	Motor's ohmic resistance	1.74
Nominal speed of motor	3000rpm	Pole pairs	4
Nominal torque of motor	2.387 Nm	Motor's torque constant	1.608 Nm/A

Fig. 8 shows a schematic of the performed simulations in Simulink environment.

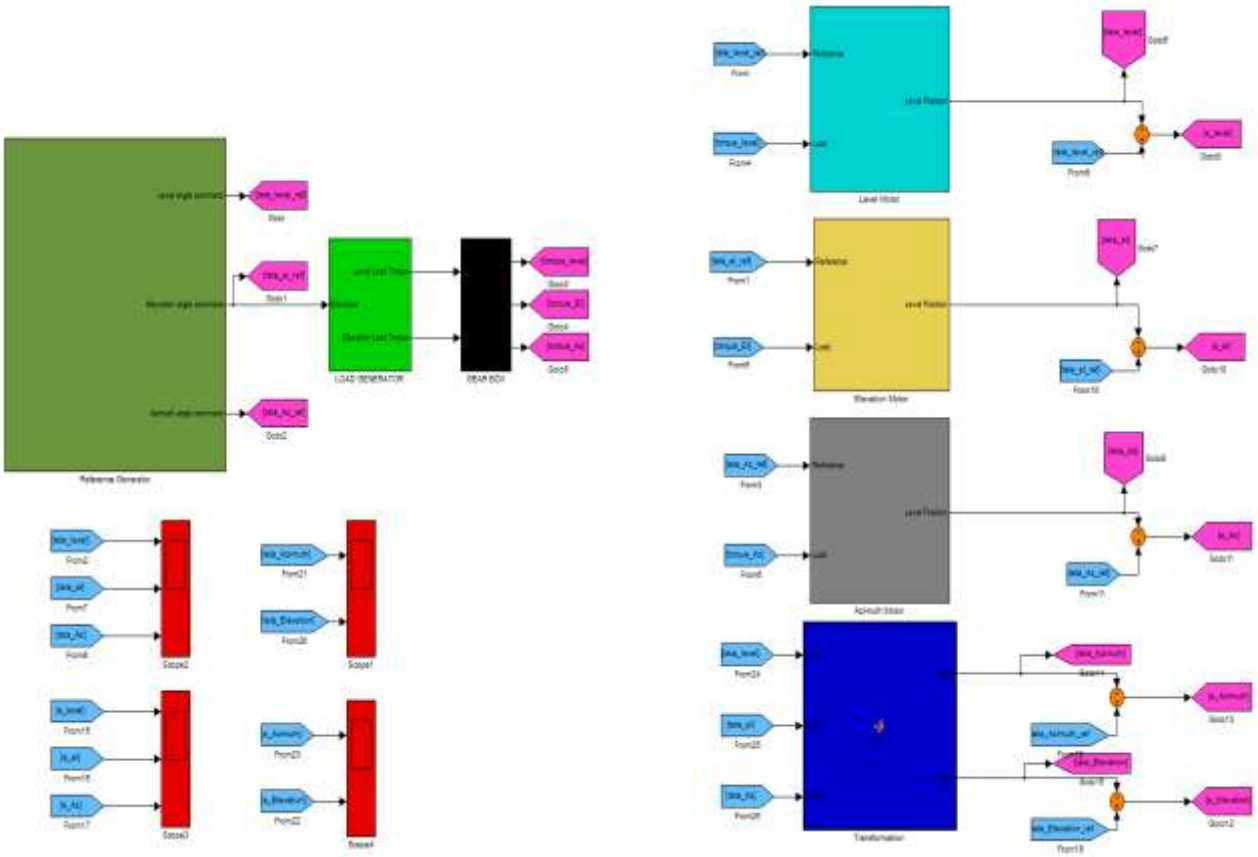

Figure 8. Schematic of implemented system in Simulink environment

The set of real data includes the interval at which the elevation angle passes the zenith angle and the azimuth angle should vary 180 degree in a short time. Figures (9) and (10) show the reference azimuth and elevation angles.

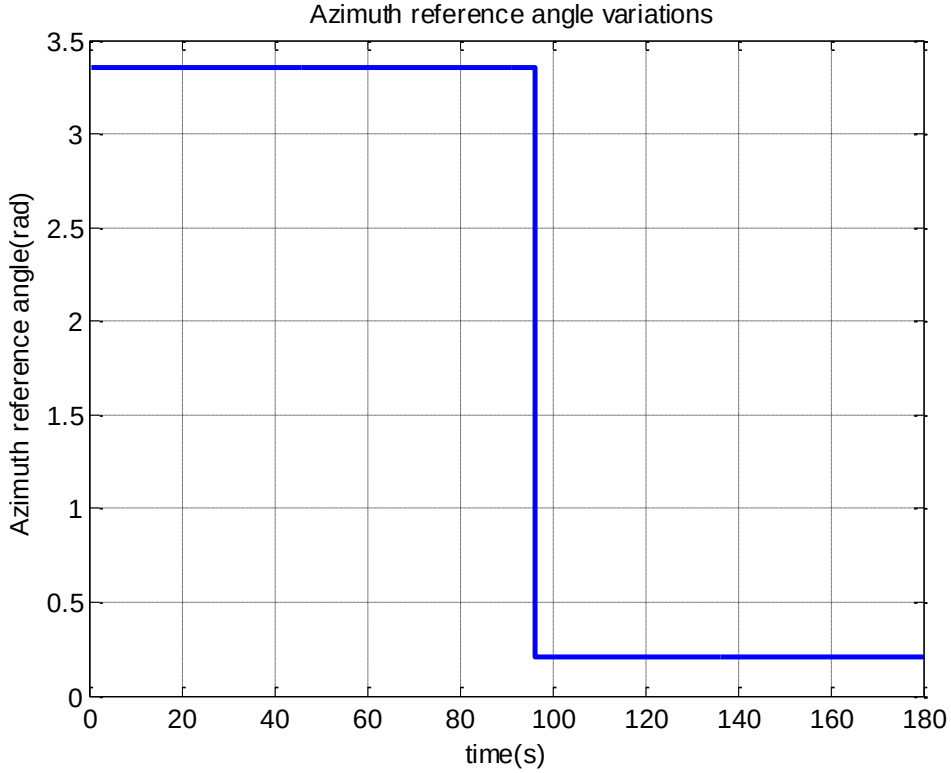

Figure 9. reference azimuth angle

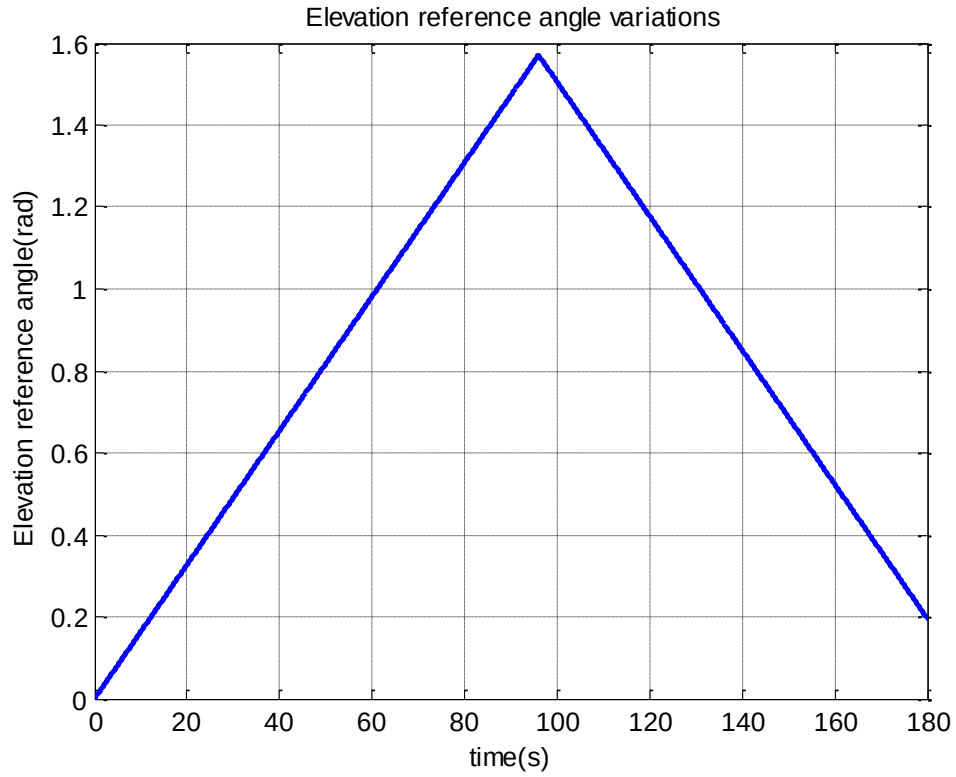

Figure 10. Reference Elevation angle variations

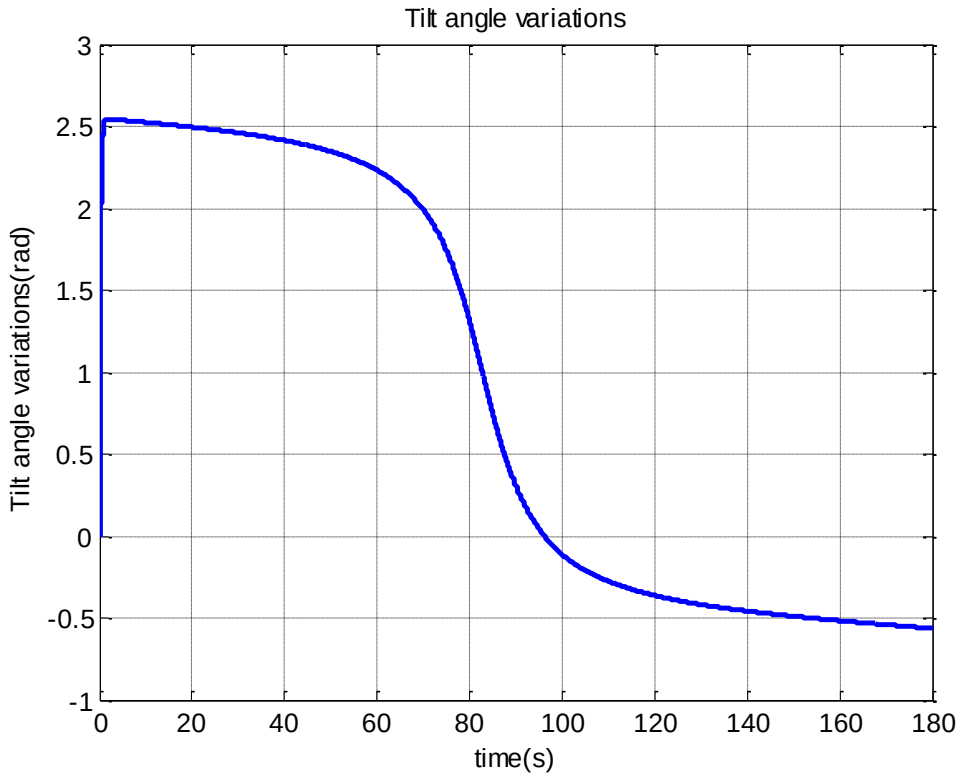

Figure 11. Variations of Tilt axis during tracking mission

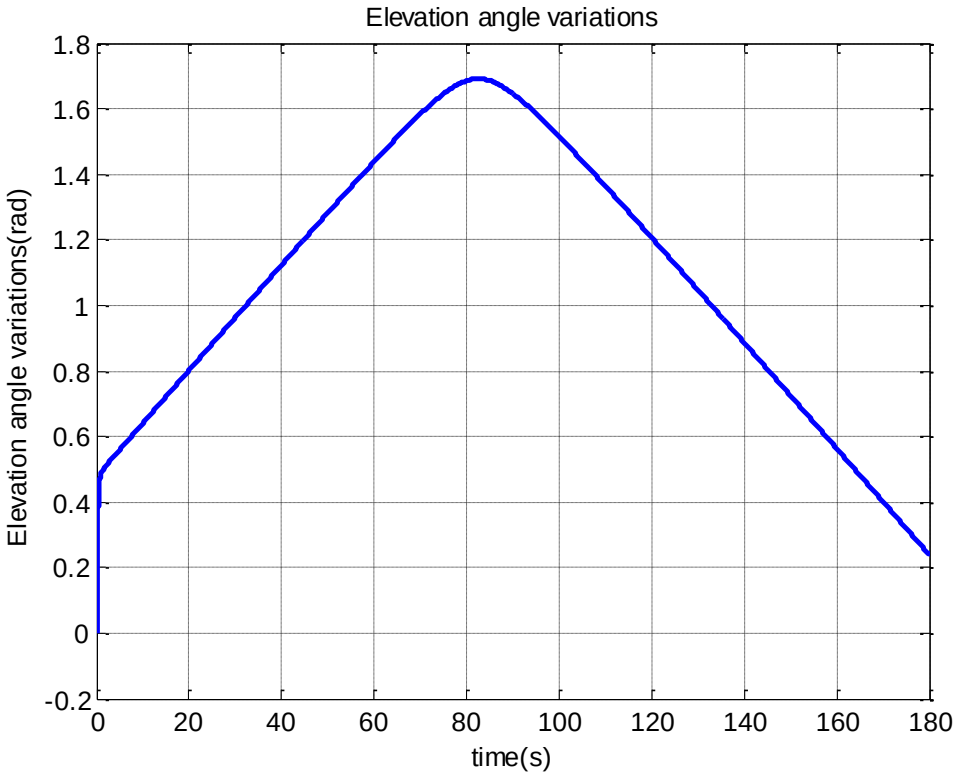

Figure 12. Variations of Elevation axis during tracking mission

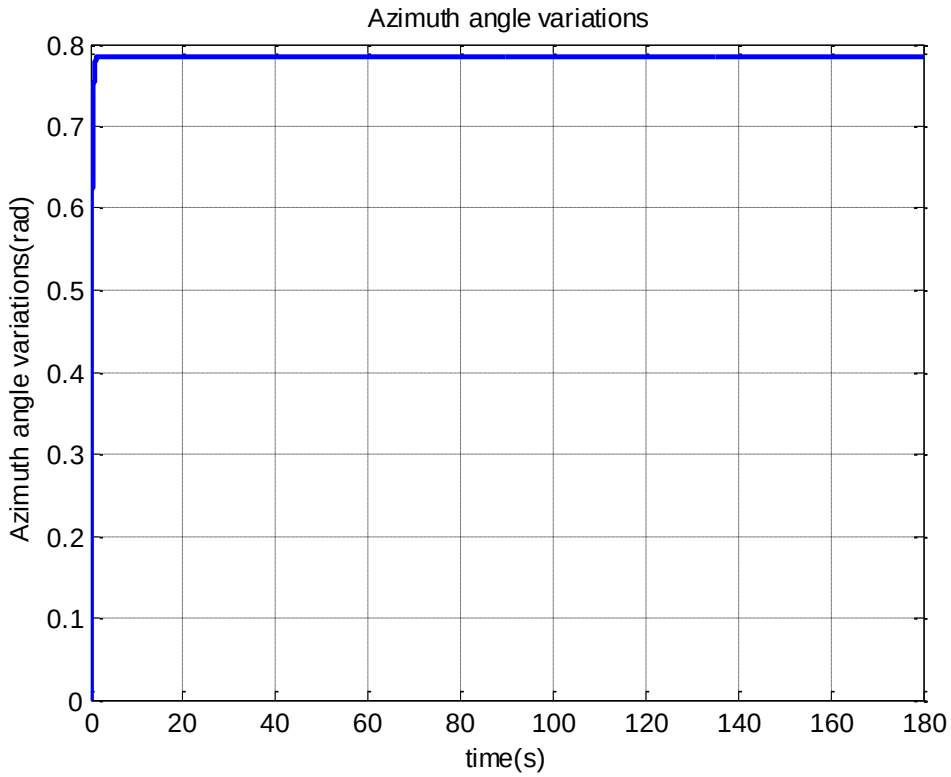

Figure 13. Variations of Azimuth axis during tracking mission

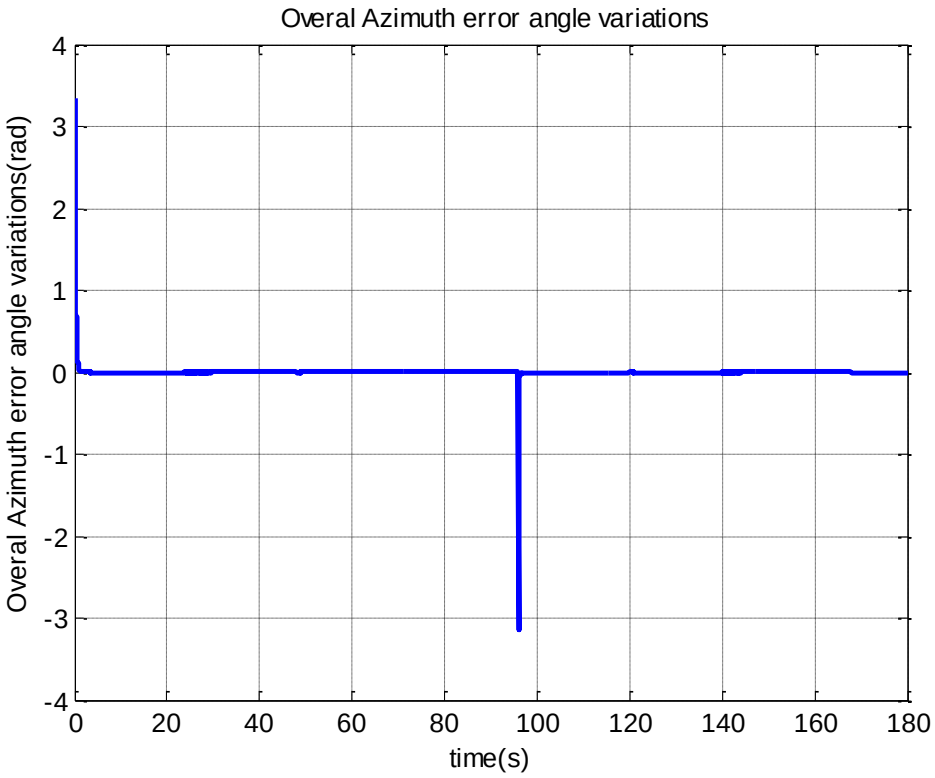

Figure 14. Difference between resultant and command azimuth angle

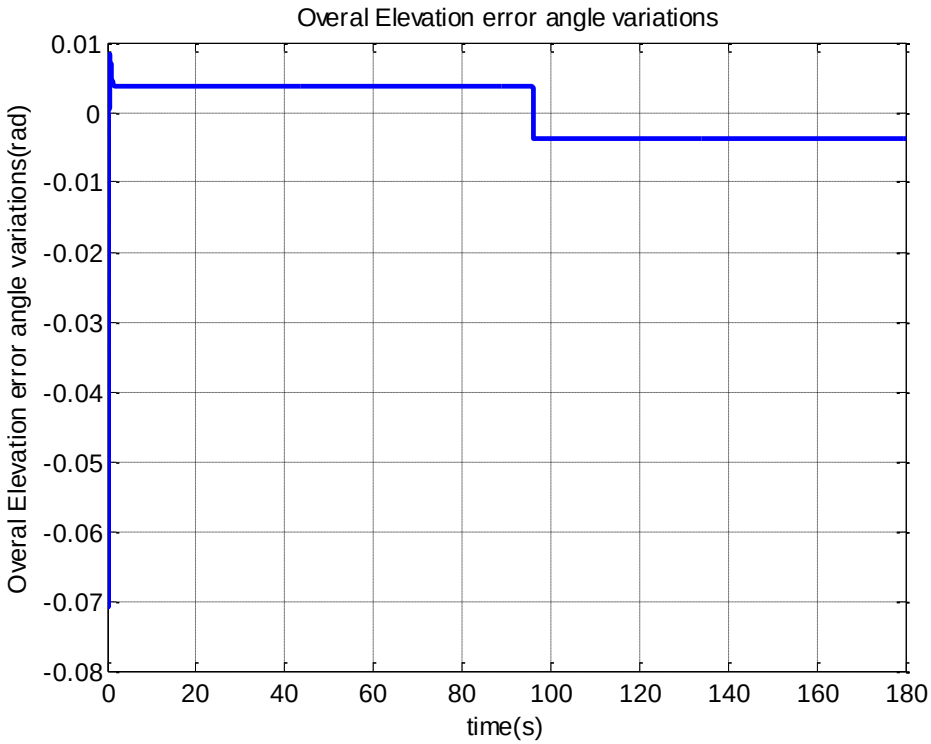

Figure 15. Difference between resultant and command Elevation angle

It should be noticed that the angles are all in radians. As it is obvious, the controllers have been successful in tracking the desired commands. The difference between real and reference azimuth angles during the sharp changes in azimuth command, is in the order of 10e-5. This results show a significant improvement in Az-El-Tilt pedestal's track, especially around the zenith point.

VI. CONCLUSION

In this paper, an Az-El-Tilt pedestal was considered to make improvements in its tracking accuracy, especially around the zenith point. The three degree of freedom pedestal system was modeled mainly by its structural components such as reflector and actuators which were chosen permanent magnet motors. After introducing a complete nonlinear model for PMSMs, a robust sliding mode position controller was developed for each of PMSMs. It was proved by simulation results that the proposed controller's performance is independent of load torque variations. The applied forces on each of the pedestal's actuator were then analyzed and the gravitational and wind forces were modeled for an Az-El-Tilt pedestal. At last, after introducing the parameters of a real pedestal and some other atmospheric conditions such as wind speed, the whole system was simulated. The output results proved effectiveness of the proposed controllers and tracking was done with a very low position error during passing the zenith point considering wind blowing and change in gravitational force distribution.

REFERENCES

[1] P.S. Crawford, "Trajectory Optimization to Minimize Antenna Pointing Error," *Computing and Control Engineering Journal*, April 1995.
[2] H. Wakana, "Fade Characteristics for K-band Land-mobile Satellite Channels in Tokyo Measured Using COMETS," Electronics Letters , Vol. 35, No.22, October 1999, pp. 1912-1913.
[3] T.S. Kelso, "Basics of the Geostationary Orbit," *Satellite Times*, Vol. 4, No. 5, May. 1998.
[4] G. Maral and M. Bousquet, Satellite Communications Systems , Third Edition, Wiley, 1998.
[5] C. Busch, P. Lancaster and E. Payne, "A Mobile 4.3 Metre Remote Sensing Ground Station Rapid Deployment and High Performance," International Telemetering Conference Proceedings (33), October 27-30, 1997.
[6] Y. X. Su, C. H. Zheng, and B. Y. Duan, "Automatic disturbances rejection controller for precise motion control of permanent-magnet synchro-nous motors, "IEEE Trans. Ind. Electron., vol. 52, no. 3, pp. 814–823, Jun. 2005.
[7] K. H. Kim and M.-J. Youn, "A nonlinear speed control for a PM synchronous motor using a simple disturbance estimation technique, "IEEE Trans. Ind. Electron., vol. 49, no. 3, pp. 524–535, Jun. 2002.
[8] B. Grcar, P. Cafuta, M. Znidaric, and F. Gausch, "Nonlinear control of synchronous servo drive," IEEE Trans. Control Syst. Technol.,vol.4, no. 2, pp. 177–184, Mar. 1996.
[9] G. J. Wang, C. T. Fong, and K. J. Chang, "Neural-network-based self-tuning PI controller for precise motion control of PMAC motors," IEEE Trans. Ind. Electron., vol. 48, no. 2, pp. 408–415, Apr. 2001.
[10] H. Z. Jin and J. M. Lee, "An RMRAC current regulator for permanent-magnet synchronous motor based on statistical model interpretation," IEEE Trans. Ind. Electron., vol. 56, no. 1, pp. 169–177, Jan. 2009.
[11] Y. A.-R. I. Mohamed, "Design and implementation of a robust current-control scheme for a PMSM vector drive with a simple adaptive disturbance observer," IEEE Trans. Ind. Electron., vol. 54, no. 4, pp. 1981–1988, Aug. 2007.
[12] Y. A.-R. I. Mohamed and E. F. El-Saadany, "A current control scheme with an adaptive internal model for torque ripple minimization and robust cur-rent regulation in PMSM drive systems, "IEEE Trans. Energy Convers., vol. 23, no. 1, pp. 92–100, Mar. 2008.
[13] T.-L. Hsien, Y.-Y. Sun, and M.-C. Tsai, "H∞control for a sensorless permanent-magnet synchronous drive,"Proc. Inst. Elect. Eng.—Electr. Power Appl., vol. 144, no. 3, pp. 173–181, May 1997.
[14] I. C. Baik, K.-H. Kim, and M. J. Youn, "Robust nonlinear speed control of PM synchronous motor using boundary layer integral sliding mode control technique," IEEE Trans. Control Syst. Technol., vol. 8, no. 1, pp. 47–54, Jan. 2000.
[15] R. J. Wai, "Total sliding-mode controller for PM synchronous servo motor drive using recurrent fuzzy neural network,"IEEE Trans. Ind. Electron., vol. 48, no. 5, pp. 926–944, Oct. 2001.
[16] B. Grcar, P. Cafuta, M. Znidaric, and F. Gausch, "Nonlinear control of synchronous servo drive," IEEE Trans. Control Syst. Technol.,vol.4, no. 2, pp. 177–184, Mar. 1996.
[17] D. M. Vilathgamuwa, M. A. Rahman, K. Tseng, and M. N. Uddin, "Non-linear control of interior permanent magnet synchronous motor," IEEE Trans. Ind. Appl., vol. 39, no. 2, pp. 408–416, Mar./Apr. 2003.
[18] J. Zhou and Y. Wang, "Adaptive backstepping speed controller design for a permanent magnet synchronous motor,"Proc. Inst. Elect. Eng.—Electr. Power Appl., vol. 149, no. 2, pp. 165–172, Mar. 2002.
[19] Y.-S. Kung and M.-H. Tsai, "FPGA-based speed control IC for PMSM drive with adaptive fuzzy control,"IEEE Trans. Power Electron., vol. 22, no. 6, pp. 2476–2486, Nov. 2007.